# Two-dimensional optical wavelet decomposition with white-light illumination by wavelength multiplexing

**José J. Esteve-Taboada, Javier García, and Carlos Ferreira**

*Departament Interuniversitari d'Òptica, Facultat de Física, Universitat de València, C/Doctor Moliner 50, 46100 Burjassot (València), Spain*

**David Mendlovic and Zeev Zalevsky**

*Faculty of Engineering, Tel Aviv University, Tel Aviv 69978, Israel*

Received November 24, 1999; revised manuscript received August 14, 2000; accepted August 15, 2000

We present a novel method for achieving in real time a two-dimensional optical wavelet decomposition with white-light illumination. The underlying idea of the suggested method is wavelength multiplexing. The information in the different wavelet components of an input object is transmitted simultaneously in different wavelengths and summed incoherently at the output plane. Experimental results show the utility of the new proposed method. © 2001 Optical Society of America

*OCIS codes:* 060.4230, 100.7410, 070.4550, 070.4560.

## 1. INTRODUCTION

The Fourier transform (FT) analysis of transient signals having short temporal (or spatial) extent usually results in high-frequency noise coming from the periodic mode contributions outside the short temporal (or spatial) extent of the signal. Many approaches have been devised to solve this problem. One of the solutions was the Gabor transform.[1] In this method the transient signal is multiplied by a window function before the Fourier analysis is performed. Although the position of the window function can be changed along the time (or space) axis, its width is fixed in both the time (or space) and frequency domains. Thus this method produces instabilities when noisy signals (such as speech or seismic signals) are analyzed.[2]

Another method that solves the problem of high-frequency noise when analyzing short temporal (or spatial) extent signals is the wavelet transform (WT).[3] This transform uses decomposition of a function according to scaled and shifted versions of a basic mother wavelet function. The WT is also well adapted to handling data compression and bandwidth reduction,[4] optical pattern recognition,[2,5,6] sound analysis,[7] representation of the human retina, representation of fractal aggregates,[8] and so on.

The one-dimensional (1-D) mother wavelet function $h(x)$ is a window function (such as a Gaussian) multiplied by a modulation term. The scaled and shifted versions are called daughter wavelet functions $h_{ab}(x)$ and are generated as

$$h_{ab}(x) = \frac{1}{\sqrt{a}} h\left(\frac{x-b}{a}\right), \tag{1}$$

where $a$ is the scale parameter, $b$ is the shift amount, and $\sqrt{a}$ is the normalization factor. The 1-D wavelet transform $W(a, b)$ of the signal $f(x)$ is defined as[9]

$$W(a, b) = \int_{-\infty}^{+\infty} f(x) h_{ab}^{*}(x) \mathrm{d}x. \tag{2}$$

Note that Eq. (2) has the form of a correlation operation between the input signal $f(x)$ and the scaled mother wavelet function $h(x)$. This fact is the basis for the optical implementation of this transform. For two-dimensional (2-D) input signals $f(x, y)$, the 2-D wavelet transform is defined as

$$W(a, \mathbf{b}) = \frac{1}{a} \int_{-\infty}^{+\infty} \int_{-\infty}^{+\infty} f(x, y) h^{*}\left(\frac{x-b_1}{a}, \frac{y-b_2}{a}\right) \mathrm{d}x \mathrm{d}y, \tag{3}$$

where

$$\mathbf{b} = \begin{pmatrix} b_1 \\ b_2 \end{pmatrix}.$$

In recent years several successful methods have been proposed in order to implement optically the WT for both 1-D and 2-D input signals. One approach is based on the VanderLugt $4f$ configuration with a multireference-matched filter (see Refs. 10 and 11). In this system every daughter wavelet is encoded with a different reference beam, and the result is several wavelet components spatially multiplexed. Another method to achieve a 2-D real-time WT is based on recycling the input through an optical correlator and using the magnification and reduction capabilities of optics to scale it.[12]

Another approach to obtain the 2-D WT in real time is proposed in Ref. 13. In this method the different wavelet scales $a$ are multiplexed with a set of fixed wavelengths and incoherently added in the output plane (the system is designed to provide all the components in the same spatial locations). The input pattern should be illuminated by many spatially coherent wavelengths. Several collinear laser beams are used to provide this multiwavelength illumination.

Recently, an experimental implementation of a continuous 2-D optical wavelet transformer with white-light illumination has been demonstrated (see Refs. 14 and 15). In this approach the different scalings of the mother wavelet function are achieved at the different wavelengths of the white-light illumination. Each wavelet component can be obtained by placing a different color filter in the output plane. The main drawback of this system is its limited range of scaling factors, because the system relays the scaling only in the scale changes that are due to $\lambda$. With the use of a monochrome CCD camera, which is sensitive to the range of the near-infrared wavelengths in addition to the visible region ($450\,\mathrm{nm} < \lambda < 1250\,\mathrm{nm}$), the obtained scaling range is 2.27.

In this paper we present a novel method to obtain a 2-D optical wavelet transformer with white-light illumination by wavelength multiplexing. We are able to simultaneously obtain in real time several 2-D wavelet components of an input function, multiplexing the information related to each different scale of the wavelet mother function in a different wavelength. An arbitrary number of components can be multiplexed in the same spatial extent of the input image. The scaling of the mother wavelet is accomplished by a diffractive optical element (DOE), and thus it is not restricted to a limited range.

In Section 2 we recall the Morlet mother wavelet function used in this experiment and explain the optical setup used to perform the 2-D WT by use of wavelength multiplexing. In Section 3 we show the basic theory of the method. In Section 4 optical results demonstrate the utility of the method introduced here. Finally, in Section 5, the main conclusions are outlined.

## 2. TWO-DIMENSIONAL OPTICAL WAVELET TRANSFORMER BY WAVELENGTH MULTIPLEXING

For the following discussion we have used the Morlet mother function.[7] The definition of the 2-D Morlet mother wavelet function is as follows:

$$h(x, y) = \exp\left(2\pi i f_0 \sqrt{x^2 + y^2}\right) \exp\left(-\frac{x^2 + y^2}{2}\right). \quad (4)$$

Its Fourier transform (FT) is

$$H(u, v) = 2\pi \exp[-2\pi^2(\sqrt{u^2 + v^2} - f_0)^2]. \quad (5)$$

This function is real and nonnegative and has a circular Gaussian ring shape. In our optical experiments we have approximated the 2-D FT of the Morlet mother wavelet function by a rectangular ring shape:

$$H(u, v) \simeq \mathrm{rect}\left(\frac{\sqrt{u^2 + v^2} - f_0}{W}\right), \quad (6)$$

where rect represents the rectangular function, $W$ being its width.

The experimental optical setup to perform the 2-D WT by use of wavelength multiplexing is the one shown in Fig. 1. The underlying idea in the proposed system is to obtain the different wavelet components with different wavelengths, i.e., wavelength multiplexing. The experimental setup can be divided in two parts: The first one, the front part up to the plane $(x_3, y_3)$, is a classical convergent correlator,[16] which in our case performs the 2-D WT [see Eq. (3)]. The input object is illuminated by a white-light point source (WLPS). The filter at plane $(x_2, y_2)$ is a DOE that contains several binary rings, with each ring corresponding to the bandpass connected with the different scales of the Morlet mother wavelet function (thus each ring performs a different wavelet component of the input object). Gratings of different spatial frequencies are plotted inside each ring. A schematic illustration of the DOE is shown in Fig. 2. Because of the WLPS illumination, every first diffraction order of these gratings (which appears at a different transversal position because of the different grating periods) is smeared according to the wavelength. In addition, each of these first orders is a different wavelet component of the input object (see Fig. 3). If the choice of the grating periods is adequate, there will be an overlapping area between the three wavelet components, which will be our region of interest (as is shown in Fig. 3). Placing a slit inside this region, we can achieve the result that every wavelet component is transmitted in a different range of wavelengths (for a given input object, we can select these ranges of wavelength by changing the lateral position of the slit). However, it is necessary to correct the chromatic dispersion at the plane

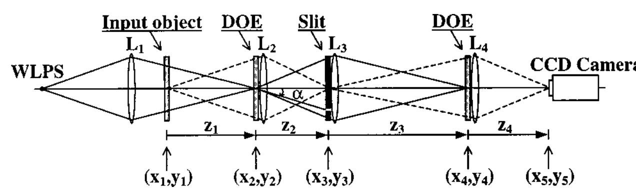


Fig. 1. Sketch of the experimental optical setup for obtaining a two-dimensional wavelet transform with white-light illumination.

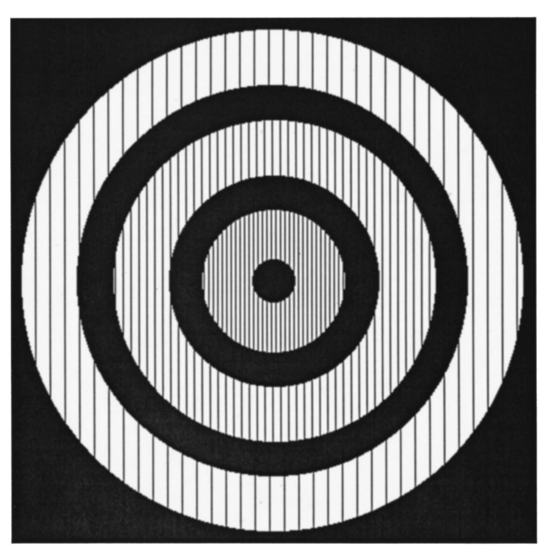

Fig. 2. Schematic illustration of the diffractive optical element.

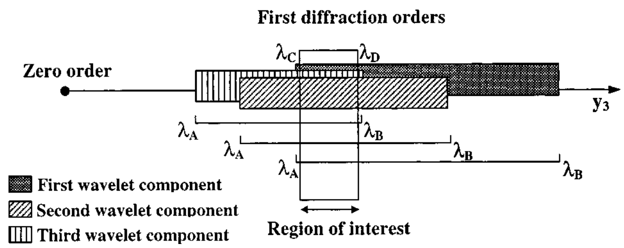


Fig. 3. Illustration of the color distribution over the plane of the slit. For graphical purposes the three chromatically dispersed wavelet components are not perfectly superimposed. With respect to the visible electromagnetic spectrum, $\lambda_A = 450$ nm and $\lambda_B = 750$ nm.

of the slit in order to obtain each wavelet component colored by its own range of wavelengths. Thus, and as we show in Section 3, the second part of the setup sketched in Fig. 1 is a system that compensates this chromatic dispersion. Lens $L_3$ provides at plane $(x_4, y_4)$ an image of the part corresponding at plane $(x_2, y_2)$ to the filtered first order at plane $(x_3, y_3)$. Another DOE, identical to the first one, placed in front of lens $L_4$, allows for the correction of the chromatic dispersion introduced by the first DOE. Finally, at plane $(x_5, y_5)$ we can obtain, incoherently added, the several wavelet components of the input object.

## 3. BASIC THEORY OF THE SYSTEM

For the sake of simplicity in the theoretical analysis of the system sketched in Fig. 1, we consider that the DOE is a single ring, so only one wavelet component of the input object will be taken into account. The extension to the complete case, which is the one optically implemented in our system, is straightforward. Also, we consider that all the distances $z_i$ $(i = 1,..., 4)$ in Fig. 1 are equal to $z$. Describing the input object by the amplitude function $s(x, y)$, we may write the distribution at plane $(x_1, y_1)$ as

$$U(x_1, y_1; \lambda) = S(\lambda)s(x_1, y_1), \tag{7}$$

where $S(\lambda)$ is the amplitude spectral distribution of the WLPS, $\lambda$ being an arbitrary wavelength. The input object $s(x_1, y_1)$ has no explicit dependence on $\lambda$, that is, its value is equal for every $\lambda$. For later use we define the object extent in the $y_1$ direction as $\Delta_y$.

Because of the lens $L_1$, at the plane of the first DOE we have the FT of the $s$ distribution, $\tilde{s}$. Immediately behind the DOE, we have, except for constant factors,

$$U(x_2, y_2; \lambda) = S(\lambda)\tilde{s}\left(\frac{x_2}{\lambda z}, \frac{y_2}{\lambda z}\right) \times H(x_2, y_2)\exp(-i2\pi y_2/T), \tag{8}$$

where $H$ represents the binary ring that is the FT of the 2-D daughter wavelet function and $T$ is the period of the grating plotted inside this ring. We have considered just the order $-1$ in the Fourier expansion of the grating, the only important one in our system, because the other orders will be filtered out.

Lens $L_2$ provides at plane $(x_3, y_3)$ the correlation between the input object function and the wavelet function, that is, the wavelet component [see Eq. (3)]. Denoting by $W$ this wavelet component, we have

$$U(x_3, y_3; \lambda) = S(\lambda)W(x_3, y_3) \otimes \delta\left(x_3, y_3 - \frac{\lambda z}{T}\right) = S(\lambda)W\left(x_3, y_3 - \frac{\lambda z}{T}\right), \tag{9}$$

where the symbol $\otimes$ denotes the convolution operation. Equation (9) is valid for all the wavelengths of the WLPS. Therefore the delta function in this equation gives the chromatic dispersion for the wavelet component at plane $(x_3, y_3)$. This expression shows that around the first diffraction order we obtain the addition of replicas of the particular wavelet component, each in a different $\lambda$ and centered at location $\lambda z/T$.

If, in this plane, we place a narrow slit centered at location $Y_0$ and with width $L$, we can achieve the result that the wavelet component is transmitted in a particular range of wavelengths. This range of wavelengths depends, as can be seen in Fig. 4(a), on the width of the slit, on the size of the wavelet component [which equals the size of the input object, owing to the unit magnification assumed between the planes $(x_1, y_1)$ and $(x_3, y_3)$], and on the value of $Y_0$. We describe the slit by the function $\mathrm{rect}[(y_3 - Y_0)/L]$, a 2-D separable function with no explicit dependence on $x$. Thus the distribution at plane $(x_3, y_3)$ is

$$U(x_3, y_3; \lambda) = S(\lambda)W\left(x_3, y_3 - \frac{\lambda z}{T}\right)\mathrm{rect}\left(\frac{y_3 - Y_0}{L}\right), \tag{10}$$

where now the value of $U(x_3, y_3; \lambda)$ is nonzero only for the wavelengths of the WLPS that pass through the slit.

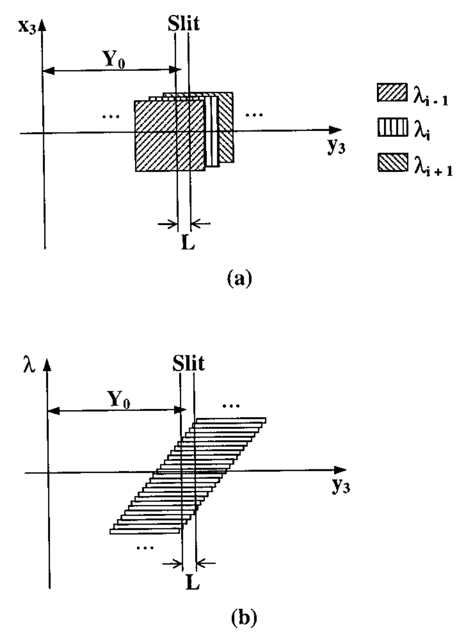


Fig. 4. (a) Chromatic dispersion at the plane of the slit for a particular wavelet component of the input object. For graphical purposes the different replicas of the wavelet component for each wavelength are not perfectly superimposed. (b) Representation of the lateral shift in the wavelet component replicas for the different wavelengths and the slit position.

This range of wavelengths will be explicitly calculated below. Note that, as can be seen in Fig. 4(a), for each of these wavelengths the slit selects a different vertical strip of the wavelet component. This is also shown in Fig. 4(b), in which a complementary representation of the plane of the slit [which consists of a cross section of plane $(x_3, y_3)$ for different wavelengths] along the $(\lambda, y_3)$ axes has been used. Thus, immediately behind the slit, we have superimposed in the same location different vertical strips of the wavelet component, each in a different wavelength.

To obtain the wavelet component colored by its particular range of wavelengths, it is necessary to correct the chromatic dispersion introduced by the first DOE. Thus, placing another DOE, identical to the first one, at plane $(x_4, y_4)$ and taking into account that the magnification between the planes $(x_2, y_2)$ and $(x_4, y_4)$ is $M = -1$, we have

$$U(x_4, y_4;\, \lambda) = S(\lambda)\left[\tilde{W}\left(\frac{x_4}{\lambda z}, \frac{y_4}{\lambda z}\right)\exp(-i2\pi y_4/T) \otimes L\,\mathrm{sinc}\left(\frac{y_4 L}{\lambda z}\right)\exp(-i2\pi Y_0 y_4)/\lambda z\right] \times \exp(i2\pi y_4/T)H(x_4, y_4), \tag{11}$$

where the exponential function $\exp(i2\pi y_4/T)$ corresponds to the order $+1$ of the Fourier expansion of the grating in the second DOE and the function $H(x_4, y_4)$ represents the binary ring that is the FT of the 2-D wavelet function of the second DOE.

Finally, lens $L_4$ provides at the plane of the camera the following result:

$$U(x_5, y_5;\, \lambda) = S(\lambda)\left[W\left(x_5, y_5 + \frac{\lambda z}{T}\right)\mathrm{rect}\left(\frac{y_5 + Y_0}{L}\right)\right] \otimes \delta\left(y_5 - \frac{\lambda z}{T}\right) \otimes h\left(\frac{x_5}{\lambda z}, \frac{y_5}{\lambda z}\right). \tag{12}$$

Taking into account the properties of the delta function, we may write this last equation as

$$U(x_5, y_5;\, \lambda) = S(\lambda)\left[W(x_5, y_5)\mathrm{rect}\left(\frac{y_5 + Y_0 - \lambda z/T}{L}\right)\right] \otimes h\left(\frac{x_5}{\lambda z}, \frac{y_5}{\lambda z}\right). \tag{13}$$

So the final result that we obtain can be understood as a strip of the wavelet component of the input object (the expression shown between square brackets) convolved with the wavelet function of the second DOE, i.e., the wavelet component of a strip of the wavelet component of the input object.

In case the rect function has the same width as that of the input object or is bigger, we get, instead of a strip of the wavelet component, the whole wavelet component of the input object convolved with the wavelet function of the second DOE. As we have used binary rings [functions $H(x_2, y_2)$ and $H(x_4, y_4)$], in this case the final result coincides with the wavelet component of the input object.

In the following explanation, for the sake of simplicity, we will assume that we are in this last case.

To clarify the result of Eq. (13), we consider the action of the rect function in the expression in square brackets. For a given position $y_5$, this function is nonzero when $|y_5 + Y_0 - \lambda z/T| \leq L/2$. In particular, considering the equality, we can obtain the maximum and minimum wavelengths that contribute to a particular position $y_5$:

$$y_5 + Y_0 - \frac{\lambda_1 z}{T} = L/2 \Rightarrow \lambda_1 = \frac{T}{z}(y_5 + Y_0 - L/2),$$

$$y_5 + Y_0 - \frac{\lambda_2 z}{T} = -L/2 \Rightarrow \lambda_2 = \frac{T}{z}(y_5 + Y_0 + L/2), \tag{14}$$

and so the width of the interval of wavelengths is

$$(\Delta\lambda)_{y5} = \lambda_2 - \lambda_1 = \frac{LT}{z}, \tag{15}$$

where $(\Delta\lambda)_{y5}$ is the interval of wavelengths that contributes to a particular position $y_5$ of the wavelet component. Note that the width of $(\Delta\lambda)_{y5}$ does not depend on the position $y_5$. This interval has a central wavelength $\lambda_{y5}$, which will be distinct for every different position $y_5$. To obtain the value of this central wavelength, we set the argument of the rect function equal to zero. This gives

$$\lambda_{y5} = \frac{T}{z}(Y_0 + y_5). \tag{16}$$

We have shown an example of this distribution of wavelengths in the plane $(x_5, y_5)$ in Fig. 5(a). In addition, we can obtain the limits of the range of central wavelengths in which the wavelet component appears. The procedure may be explained as follows: The object extent is $\Delta_y$; therefore, because of the unit magnification assumed between the planes $(x_1, y_1)$ and $(x_5, y_5)$, the maximum extension of the wavelet component $W(x_5, y_5)$ will be $\Delta_y$. Consequently, the limits of the range of central wave-

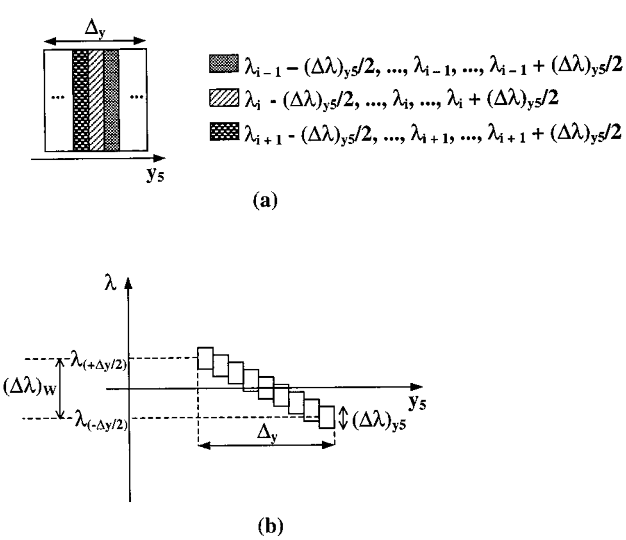


Fig. 5. (a) Output plane considering a slit represented by a rect function and (b) the same output plane as that in (a) but using the complementary representation at axes $(\lambda, y_5)$.

lengths may be calculated by replacing the value of $y_5$ in Eq. (16) by its extreme values $-\Delta_y/2$ and $\Delta_y/2$:

$$\lambda_{(-\Delta_y/2)} = \frac{T}{z}\left(Y_0 - \frac{\Delta_y}{2}\right), \qquad \lambda_{(\Delta_y/2)} = \frac{T}{z}\left(Y_0 + \frac{\Delta_y}{2}\right). \tag{17}$$

And therefore the range of central wavelengths in which the wavelet component appears is

$$(\Delta\lambda)_W = \lambda_{(\Delta_y/2)} - \lambda_{(-\Delta_y/2)} = \frac{\Delta_y T}{z}, \tag{18}$$

which is independent of the slit width.

If we take into account the interval of wavelengths for each position $y_5$ [see Eq. (15)], the total interval of wavelengths in which the wavelet component appears is $(\Delta\lambda)_W + (\Delta\lambda)_{y5}$. This is illustrated in Fig. 5(b), which shows a cross section for different wavelengths of the final plane when a rectangular slit is used. In this figure we depict the definitions of the wavelength intervals $(\Delta\lambda)_{y5}$ and $(\Delta\lambda)_W$.

Next we show some numerical results. For instance, if we consider the extension of the input object $\Delta_y = 5\,\mathrm{mm}$, the period of the grating $T = 8\,\mu\mathrm{m}$, the distances $z = 500\,\mathrm{mm}$, and the width of the slit $L = 3\,\mathrm{mm}$, the interval of wavelengths for every different position $y_5$ is [taking into account Eq. (15)] $(\Delta\lambda)_{y5} = 48\,\mathrm{nm}$, and the width of the interval of central wavelengths is [following Eq. (18)] $(\Delta\lambda)_W = 80\,\mathrm{nm}$. Therefore the total range of wavelengths is $(\Delta\lambda)_W + (\Delta\lambda)_{y5} = 128\,\mathrm{nm}$.

Let us consider now the particular case when an infinitely narrow slit is used. The slit can be represented by a delta function $\delta(y_3 - Y_0)$, a 2-D separable function with no explicit dependence on $x$. Analogously to the previous case, we can obtain the distribution at plane $(x_5, y_5)$:

$$U(x_5, y_5; \lambda) = S(\lambda)\left[W(x_5, y_5)\,\delta\left(y_5 + Y_0 - \frac{\lambda z}{T}\right)\right] \otimes h\left(\frac{x_5}{\lambda z}, \frac{y_5}{\lambda z}\right). \tag{19}$$

This case is the particular one in which the interval $(\Delta\lambda)_{y5} = 0$, so we can show that the final image has each vertical line with a different wavelength varying continuously from left to right. This particular case is the one depicted in Fig. 6(a). Figure 6(b) also shows this particular case but uses the complementary representation at axes $(\lambda, y_5)$.

Finally, we explain an important feature of the system: the relation between the size of the slit in the plane $(x_3, y_3)$ and the light source needed to obtain a reconstructed image in the plane $(x_5, y_5)$. We can consider three possible cases:

1. The slit is bigger than the size of the wavelet component. The reconstruction of the image is done in a certain spectral region, as shown in Fig. 5(a). In this case, using a light source with a single wavelength (a laser, for instance), one can obtain a complete image of the wavelet component in the final plane (this case is the one discussed in Ref. 13). The value of the wavelength needed in the light source may be selected by changing the lateral position of the slit.

2. The slit is smaller than the size of the wavelet component. Again the reconstruction of the image is done by following Fig. 5(a). In this case not all of the whole wavelet component can go through the system with a single wavelength.

3. The last case is the limiting one in which the slit is represented by a delta function. Each vertical line of the final image is reconstructed in a different wavelength [as is shown in Fig. 6(a)]. This case may be used for encoding of spatial information (such as different spatial positions and/or different spatial frequencies) in different wavelengths.

In summary, the final image of the input object is obtained in the output plane with a range of wavelengths that depends on the width and the position of the slit and on the spatial extent of the object. Choosing these parameters properly, one can use an interval in the wavelength spectrum smaller than the total spectrum width.

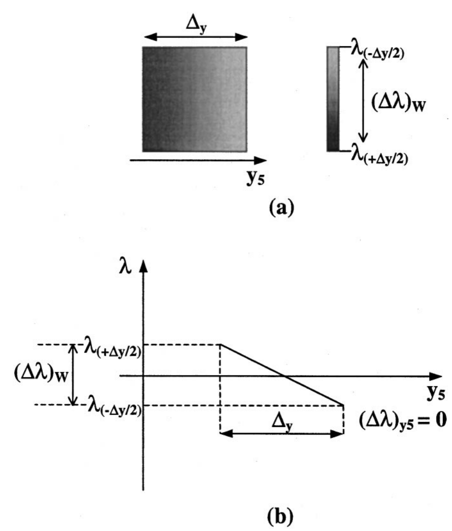


Fig. 6. (a) Output plane considering a slit represented by a delta function and (b) the same output plane as that in (a) but using the complementary representation along the $(\lambda, y_5)$ axes.

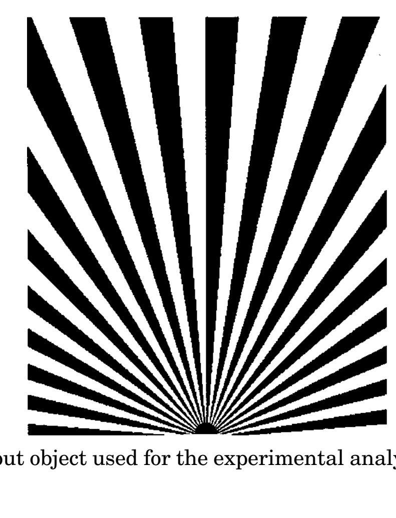

Fig. 7. Input object used for the experimental analysis of the optical setup.

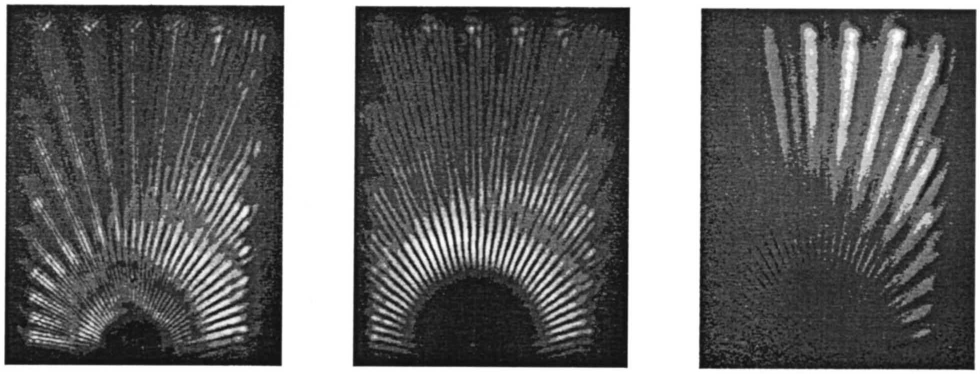

(a) (b) (c)

Fig. 8. Output results obtained for a defined position of the slit in the (a) R channel of the color camera, (b) G channel of the color camera, and (c) B channel of the color camera.

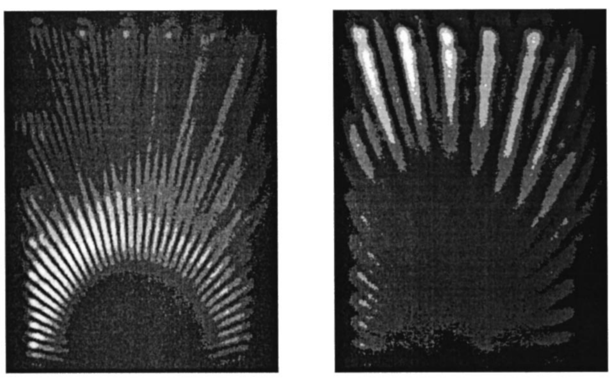

(a) (b)

Fig. 9. Output results obtained for a different position of the slit in the (a) R channel of the color camera and (b) G channel of the color camera.

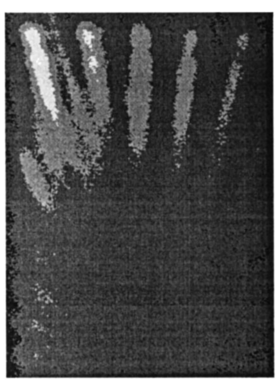

Fig. 10. Output result obtained for another different position of the slit in the R channel of the color camera.

This allows for multiplexing different wavelet components in different spectral ranges when the width of the slit is bigger than or equal to the size of the input object.

## 4. EXPERIMENTAL IMPLEMENTATION

The usefulness of the method has been tested by an optical experiment. The actual setup is the one sketched in Fig. 1. The lenses in the arrangement are as follows: $L_1$ is a 300-mm-focal-length achromatic doublet, $L_2$ and $L_3$ are achromatic photographic lenses of 135-mm focal length, and $L_4$ is a 200-mm-focal-length achromatic doublet. We have employed a 250-W xenon lamp as the white-light source. The light from this lamp has been focused onto a pinhole to form the WLPS. The input object is a piece of the rosetta pattern, as is shown in Fig. 7. The DOE's were printed with a Scitex Dolev plotter and photoreduced on a lithographic film. The periods of the gratings in the DOE's are as follows (from the inner ring to the outer one): $T_1 = 7.52\,\mu\text{m}$, $T_2 = 9.06\,\mu\text{m}$, and $T_3 = 10.72\,\mu\text{m}$. These values ensure that there will be an overlapping area between the three wavelet components in the plane $(x_3, y_3)$ (as is shown in Fig. 3). This area goes from $\alpha_1 = 3.43°$ to $\alpha_2 = 4.01°$ (for the definition of the angle $\alpha$, see Fig. 1). Analogously, as a result of the chromatic dispersion present in the plane $(x_3, y_3)$, we can refer to the overlapping area by the values of the wavelengths (denoted by $\lambda_C$ and $\lambda_D$ in Fig. 3). Thus, for the first wavelet component, these values correspond to $\lambda_C = 450\,\text{nm}$ and $\lambda_D = 526\,\text{nm}$, for the second component the values are $\lambda_C = 542\,\text{nm}$ and $\lambda_D = 634\,\text{nm}$, and for the third one the values are $\lambda_C = 642\,\text{nm}$ and $\lambda_D = 750\,\text{nm}$.

To obtain the different wavelet components in the experimental output at plane $(x_5, y_5)$, we have several options. We might use, such as in Ref. 15, a set of colored filters in order to get each wavelet component separately. However, this method requires the mechanical action of changing each colored filter for obtaining each wavelet component. Thus we have employed a better solution. Owing to the fact that in our case each wavelet component is transmitted in a different range of wavelengths, we can use a 3CCD color camera to automatically obtain the three wavelet components separately, each in a different chromatic channel of the color camera. Thus we have used a Sony DXC-950P 3CCD color video camera to grab the experimental output at plane $(x_5, y_5)$. Placing a slit of the same size as that of the input object in the suitable lateral position, we can obtain a different wavelet component in each RGB channel of the color camera (see Fig. 8). Figures 8(a), 8(b), and 8(c) show the R, G, and B channels, respectively, of the output from the color camera. We can see how the high frequencies appear only in the R channel, the medium frequencies show up principally in the G channel, and the low frequencies appear only in the B channel (the medium frequencies that appear in the R channel are due to the relatively smooth fall in the spectral response of the red CCD filter in the range of green wavelengths).

As stated above, for a given input object we can choose the range of wavelengths in which each wavelet component appears by changing the lateral position of the slit. Thus, moving it away from the zero order, we can obtain the results shown in Fig. 9. Figures 9(a) and 9(b) show the R and G channels, respectively, of the color camera. Now we can see how the low frequencies appear only in the G channel and the medium frequencies appear in the R channel (the high frequencies are now in the range of the near-infrared spectrum, and thus the color camera does not detect it). In this case, the B channel of the color camera does not contain information about the input object. Finally, moving the slit again in the same direction, we can obtain the results shown in Fig. 10. In this figure, only the R channel of the color camera is depicted. Now the low frequencies appear in the R channel, and the medium and high frequencies are both in the range of the near-infrared spectrum. In this case the G and B channels of the color camera do not contain any wavelet component of the input object.

## 5. CONCLUSIONS

In this paper we have presented a novel method for achieving in real time a 2-D optical wavelet transform with white-light illumination. The method is based on the wavelength multiplexing idea: the use of several wavelengths to transmit simultaneously the information related to different 2-D wavelet components of the input object. An arbitrary number of components (according to the number of rings in the filter) can be multiplexed in the same spatial extent of the input image. At the output plane the information transmitted by means of the different wavelengths is added incoherently, and the original input object may be formed. This method of wavelet component multiplexing can be successfully used for both image processing and communication transmittance applications. Note that the demonstrated experiment was performed with the Morlet mother wavelet function, but obviously, other mother functions may be used as well.

## ACKNOWLEDGMENTS

José J. Esteve-Taboada acknowledges a grant from the Conselleria de Cultura, Educació i Ciència (Generalitat Valenciana). This work has been supported by the Spanish Ministerio de Educación y Cultura under project PB96-1134-C02-02.

Corresponding author: José J. Esteve-Taboada, Departament d'Òptica-Universitat de València, C/ Doctor Moliner 50, 46100 Burjassot (València) Spain. Phone, 34-96-386-43-43; fax, 34-96-386-47-15; e-mail, Jose.J.Esteve@uv.es.

## REFERENCES


1. D. Gabor, "Theory of communication," J. Inst. Electr. Eng. **93**, 429–457 (1946).
2. H. Szu, Y. Sheng, and J. Chen, "Wavelet transform as a bank of matched filters," Appl. Opt. **31**, 3267–3277 (1992).
3. J. M. Combes, A. Grossmann, and Ph. Tchamitchian, eds., *Wavelets: Time Frequency Methods and Phase Space*, 2nd ed. (Springer-Verlag, Berlin, 1990).
4. J. Caulfield and H. Szu, "Parallel discrete and continuous wavelet transforms," Opt. Eng. **31**, 1835–1839 (1992).
5. X. J. Lu, A. Katz, E. G. Kanterakis, and N. P. Caviris, "Joint transform correlation using wavelet transforms," Opt. Lett. **17**, 1700–1703 (1992).
6. R. A. Maestre, J. García, and C. Ferreira, "Pattern recognition using sequential matched filtering of wavelet coefficients," Opt. Commun. **133**, 401–414 (1997).
7. R. K. Martinet, J. Morlet, and A. Grossmann, "Analysis of sound patterns through wavelet transforms," Int. J. Pattern Recogn. Artif. Intell. **1**, 273–302 (1987).
8. E. Freysz, B. Pouligny, F. Argoul, and A. Arneodo, "Optical wavelet transform of fractal aggregates," Phys. Rev. Lett. **64**, 7745–7748 (1990).
9. I. Daubechies, "The wavelet transform time–frequency localization and signal analysis," IEEE Trans. Inf. Theory **36**, 961–1005 (1990).
10. D. Mendlovic, I. Ouzieli, I. Kiryuschev, and E. Marom, "Two-dimensional wavelet transform achieved by computer-generated multireference matched filter and Dammann grating," Appl. Opt. **34**, 8213–8219 (1995).
11. D. Mendlovic and N. Konforti, "Optical realization of the wavelet transform for two-dimensional objects," Appl. Opt. **32**, 6542–6546 (1993).
12. M. O. Freeman, A. Fedor, B. Bock, and K. A. Duell, "Optical wavelet processor for producing spatially-localized, ring-wedge-type information," in *Optical Information Processing Systems and Architectures IV*, B. Javidi, ed., Proc. SPIE **1772**, 241–250 (1992).
13. J. García, Z. Zalevsky, and D. Mendlovic, "Two-dimensional wavelet transform by wavelength multiplexing," Appl. Opt. **35**, 7019–7024 (1996).
14. D. Mendlovic, "Continuous two-dimensional on-axis optical wavelet transformer and wavelet processor with white-light illumination," Appl. Opt. **37**, 1279–1282 (1998).
15. Z. Zalevsky, "Experimental implementation of a continuous two-dimensional on-axis optical wavelet transformer with white-light illumination," Opt. Eng. **37**, 1372–1375 (1998).
16. J. W. Goodman, *Introduction to Fourier Optics*, 2nd ed., Electrical Engineering Series (McGraw-Hill, Singapore, 1996).